EFFECTS OF MICROSTRUCTURE ON THE SUBSURFACE CRACK INITIATION OF TI-6AL-4V ALLOYS

O. Umezawa, K. Nagai, H. Yokoyama* and T. Suzuki*

National Research Institute for Metals
1-2-1 Sengen, Tsukuba, Ibaraki 305, Japan
* Department of Mechanical Engineering, Kogakuin University
Nishi-shinjyuku, Shinjyuku, Tokyo 163-91, Japan

Abstract

In order to clarify how the subsurface crack initiation site generates according to microstructure in high-cycle fatigue, Ti-6Al-4V alloys with different microstructures were subjected to fatigue test in liquid nitrogen. Microstructure influenced the S-N curves in long-life range. The subsurface crack initiation site was a facet or its aggregate which originated from the α grain transgranular cracking in each material. The size of subsurface crack initiation site highly depended on the maximum cyclic stress range.

High Cycle Fatigue of Structural Materials
(In Honor of Professor Paul C. Paris)
Edited by W.O. Soboyejo and T.S. Srivatsan
The Minerals, Metals & Materials Society, 1997

Introduction

Subsurface (internal) crack initiation in high cycle fatigue is usually associated with the presence of inclusions or pores.[1] In Ti-6Al-4V alloy, however, the subsurface crack initiation not associated with the pre-existing defects has been often reported regardless of testing and metallurgical conditions, i.e. temperature, frequency, stress ratio $R=\sigma_{min}/\sigma_{max}$, environment, manufacturing process, impurities concentration and microstructure.[2-10] Comparison of S-N data among the literatures has some difficulties, since most of the fatigue tests were interrupted within 10^8 cycles and few analyses were done for the site characterization. Available data under cyclic axial loading condition have been almost limited for the references listed in Table I.

According to the summarized results in Table I, the subsurface crack initiation has been detected in lower peak stress and/or in longer-life range over 10^5 cycles. The morphology of subsurface crack initiation site in the alloys could be associated with their microstructure. The effects of frequency, environment and specimen surface condition can be hardly detected on the S-N curve in the region of subsurface crack initiation. However, the mean stress possibly plays a major role on the subsurface crack initiation behavior.[6,11] Under R= -1 condition, the subsurface crack initiation is difficult to detect at or below 10^7 cycles.[6] Cryogenic temperature fatigue is most favorable to characterize the subsurface crack generation, since the subsurface crack initiation prevails more at lower temperature supposedly due to higher static strength and is detected shorter cycles to failure below at 77 K than at room temperature.[12]

In Ti-6Al-4V alloy, the materials having various microstructures such as equiaxed, bi-modal, acicular, lamella, and Widmanstäten, can be easily obtained by heat-treatments. Influence of microstructure on fatigue behavior has been pointed out; Peters et al. [13,14] reported that a fine structure exhibited a better fatigue strength in long-life regime, and that the fatigue strength was related with the texture; The fatigue strength at the long-life over 10^6 cycles in the subsurface crack initiation regime depended on not only the tensile strength but also the microcrack growth behavior.[15] However, few systematic studies have been available concerning the subsurface fatigue crack initiation and fatigue strength in long-life regime.

In the present study, therefore, the subsurface fatigue crack initiation of Ti-6Al-4V alloys at 77 K has been investigated in order to clarify the effect of microstructure on fatigue behavior in long-life range.

Experimental Procedures

Materials

A Ti-6Al-4V alloy in mill-annealed plate, *Normal2*, was heat-treated differently to achieve the different microstructures; *$\alpha+\beta$ annealed* materials were heated for 3.6 ks at 1273 K (below β-transus temperature) followed by air-cooling (H1) or water-quenching (H2); *β annealed* materials were heated for 3.6 ks at 1323 K (above β-transus temperature) followed by furnace-cooling (H3), air-cooling (H4) or water-quenching (H5). Furthermore, the fatigue fractured specimens of Ti-6Al-4V alloys in the previous study, i.e. *Normal*, *ELI*, and *Sp.ELI*, [10] were also involved for the characterization of their subsurface crack initiation sites. The *Normal*, *ELI* and *Sp.ELI* alloys were subjected to two kinds of processing: namely forging alone and

Table I Subsurface Crack Initiation in High-cycle Fatigue of Ti-6Al-4V Alloys and Its Origin

Materials	Stress ratio, R	Environment	Cycles range appeared subsurface fracture	Subsurface crack origin	References
IMI 318	0	dry argon, air, H_2O saturated air	10^7 - $3x10^7$	cleavage facet (α phase)	[3]
mill-annealed bar	-1, 0	air	10^6 - 10^8	cleavage $(001)_\beta$	[4]
mill-annealed bar	0	air, NaCl solution	10^7 - 10^{10}	undetermined	[2]
bi-modal	-1, 0.2	vacuum, air	10^6 - 10^7 / R=0.2	undetermined	[6]
fine lamellar	-1, 0.2	vacuum, air	10^6 -10^7 / R=0.2	undetermined	[6]
coarse acicular	-1, 0	air	10^6 - 10^8	cleavage $(001)_\beta$ / colony facet	[4],[5]
Widmanstätten	-1, 0	air	10^6 - 10^8	cleavage $(001)_\beta$ / colony facet	[4],[5]
as cast	0.1	air	$5x10^4$ - $2x10^5$	pore	[7]
cast + HIP	0.1	air	$2x10^5$ - 10^6	facet (α colony / GB α)	[8]
P/M	0.1	air	$4x10^5$ - 10^7	facet (α phase)	[9]
mill-annealed bar	0.01	liquid helium	10^5 - $3x10^6$	transgranular (α grain)	[10]
	0.01	liquid nitrogen	10^5 - 10^7	transgranular (α grain)	[10]
	0.01	air	10^5 - 10^7	transgranular (α grain)	[10]

HIP: hot isostatically press

P/M: powder metallurgy

GB α: grain boundary α

forging + rolling. These processed alloys were designated as *forged* material and *rolled* one, respectively. In both processes the materials were heated at 1173 K and materials were finally mill-annealed. In the *rolled* material, the reduction ratio in section area was eight times that of the *forged* material. Their chemical compositions and tensile properties are given in Table II and III.

Table II Chemical Compositions of Test Materials

Alloys	Concentration							
	Al	V	Fe	O	N	H	C	Ti
Normal 2	6.20	4.06	0.074	0.171	0.0081	0.0010	-	bal.
Normal	6.34	4.23	0.199	0.135	0.0071	0.0053	0.011	bal.
ELI	6.23	4.25	0.200	0.104	0.0035	0.0032	0.011	bal.
Sp.ELI	5.97	4.12	0.028	0.054	0.0019	0.0055	0.024	bal.

Table III Tensile properties of Test Materials

Materials		Ultimate tensile strength (MPa)	Elongation (%)
annealed	H1	1396	11.9
	H2	1430	9.7
	H3	1368	5.0
	H4	1355	5.1
	H5	1363	7.8
forged	Normal	1573	12.1
	ELI	1502	13.8
	Sp.ELI	1427	12.2
rolled	Normal	1634	10.1
	ELI	1576	13.5
	Sp.ELI	1438	12.2

Figure 1 represents the SEM secondary images of microstructure for the *annealed* materials. The H1 and H2 have the equiaxed α grain structure. The α grain diameter is from 5 to 10 μm. The H3 and H4 exhibit the lamella-like microstructure. The α plate in H3 is coarse and its width is from 5 to 10 μm. The α grain width of H4 is about 1 μm. The H5 shows the Widmanstäten α grain structure. The prior-β grain (colony) structure was observed in H3, H4 and H5, and its size in each material was about a few hundred micron-meter. The prior-β grain structure is divided into several packet structures where α platelet is aligned as shown in Figure 1(c). The *forged* materials were principally composed of elongated α grains and β platelet; they had a region in which α grains were aligned as a packet structure. The mean width of α grains was 5.0, 4.0 and 1.9 μm in *Normal*, *ELI* and *Sp.ELI*, respectively. The *rolled* materials

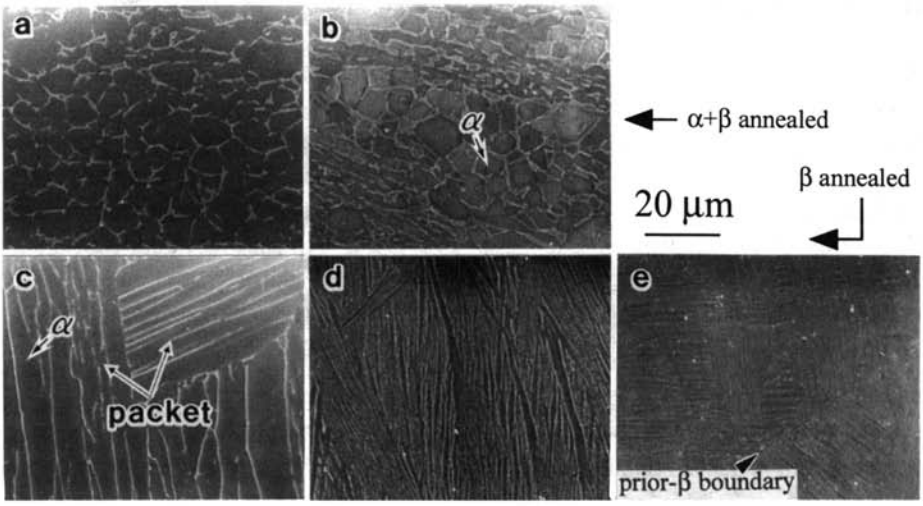

Figure 1 Microstructure of *annealed* materials: (a) H1, (b) H2, (c) H3, (d) H4 and (e) H5.

were composed of globular α grains and fine β particles. The mean diameter of α grains was 4.0, 4.0 and 2.8 μm in *Normal*, *ELI* and *Sp.ELI*, respectively. Some details of the *forged* and *rolled* materials were described in elsewhere.[10,12]

Fatigue Test

Unnotched round-bar specimens of 15 mm in gauge length and 3 mm in gauge diameter were machined in the L-direction from each *annealed* material. Fatigue tests were carried out for the specimen emersed in liquid nitrogen (77 K). Using a servo-hydraulic fatigue test machine, load-controlling tests were performed with a stress ratio, R= 0.01, and a sinusoidal waveform. The test frequency was 10 Hz until 10^6 cycles and then was accelerated up to 20 Hz. The fatigue tests were interrupted with a maximum of about $2x10^7$ cycles.

Characterization of Subsurface Crack Initiation Site

SEM observation was performed to study the fatigue crack initiation site and microcracks in specimens. Generally the main crack (Stage II) propagates almost perpendicular to the principal stress axis. On the other hand, the subsurface crack initiation site is inclined (several ten degree) against the principal stress axis. In this study, the whole of the inclined area (Stage I) is regarded as the subsurface crack initiation site, and the minor axis of an orthographic projection of the site on the main crack propagating plane is adopted as a crack length parameter, fs, to quantify the size of the subsurface crack initiation site. One of the major reasons why the minor axis is adopted is that the axis is almost parallel to the initial propagating direction of the main crack.

Results and Discussion

S-N Curves and Crack-initiation Location

Figure 2 shows all S-N curves of the test materials with normalizing the peak stresses by the tensile strength at 77 K. Most of the materials clearly exhibited two kinds of fatigue crack initiation: namely subsurface crack initiation and surface one. It is revealed that the crack initiation site shifts from the specimen surface to the specimen interior at about 0.7 in the ratio of fatigue strength. Such change of the crack initiation mechanism introduces a plateau ("knee") followed by a rather sharp drop in the shape of S-N curve as shown in Figure 2 (c) and (d). The H1 and H2 have a higher fatigue strength than the H3 and H4 in the number of cycles between 10^5 and 10^6. However, the normalized 10^7 cycles fatigue strength of the *β annealed* materials (H3, H4 and H5) is about 0.4 and superior to that of the *α+β annealed* materials (H1 and H2). The rolled materials exhibit higher normalized fatigue strength at 10^7 cycles.

The subsurface crack initiation sites were mostly placed close to the specimen surface, i.e. 10-200 μm in depth, regardless of peak cyclic stress.[16] For the β-annealed materials, a few deeper cases, i.e. about 700 μm in depth, were seen.

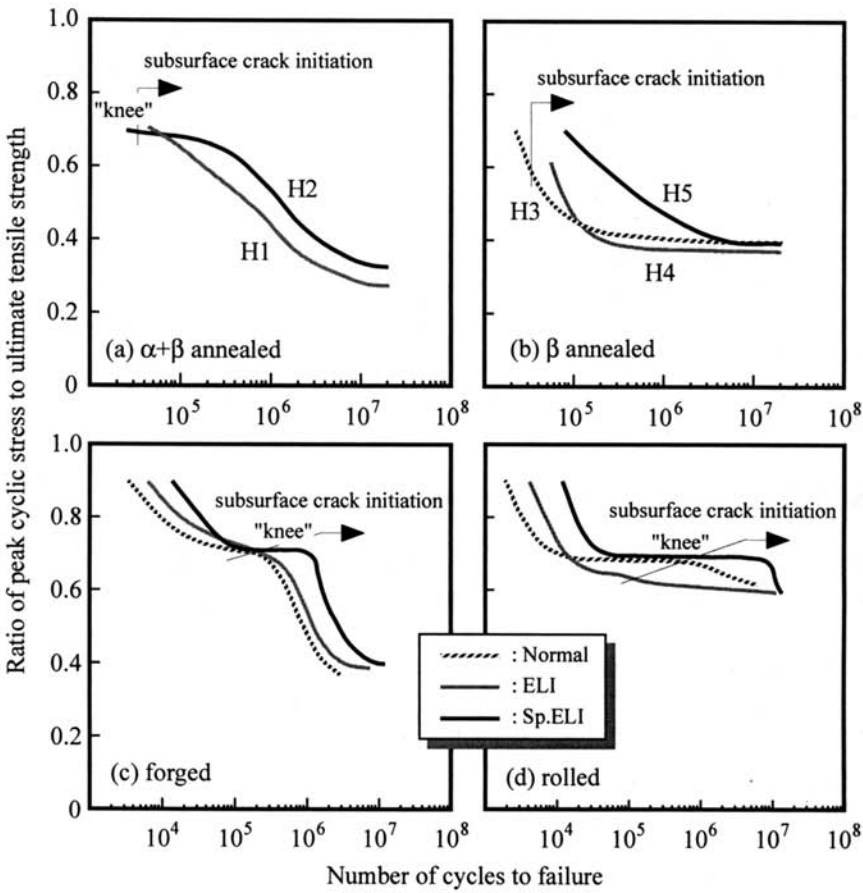

Figure 2 S-N curves of Ti-6Al-4V alloys at 77 K.

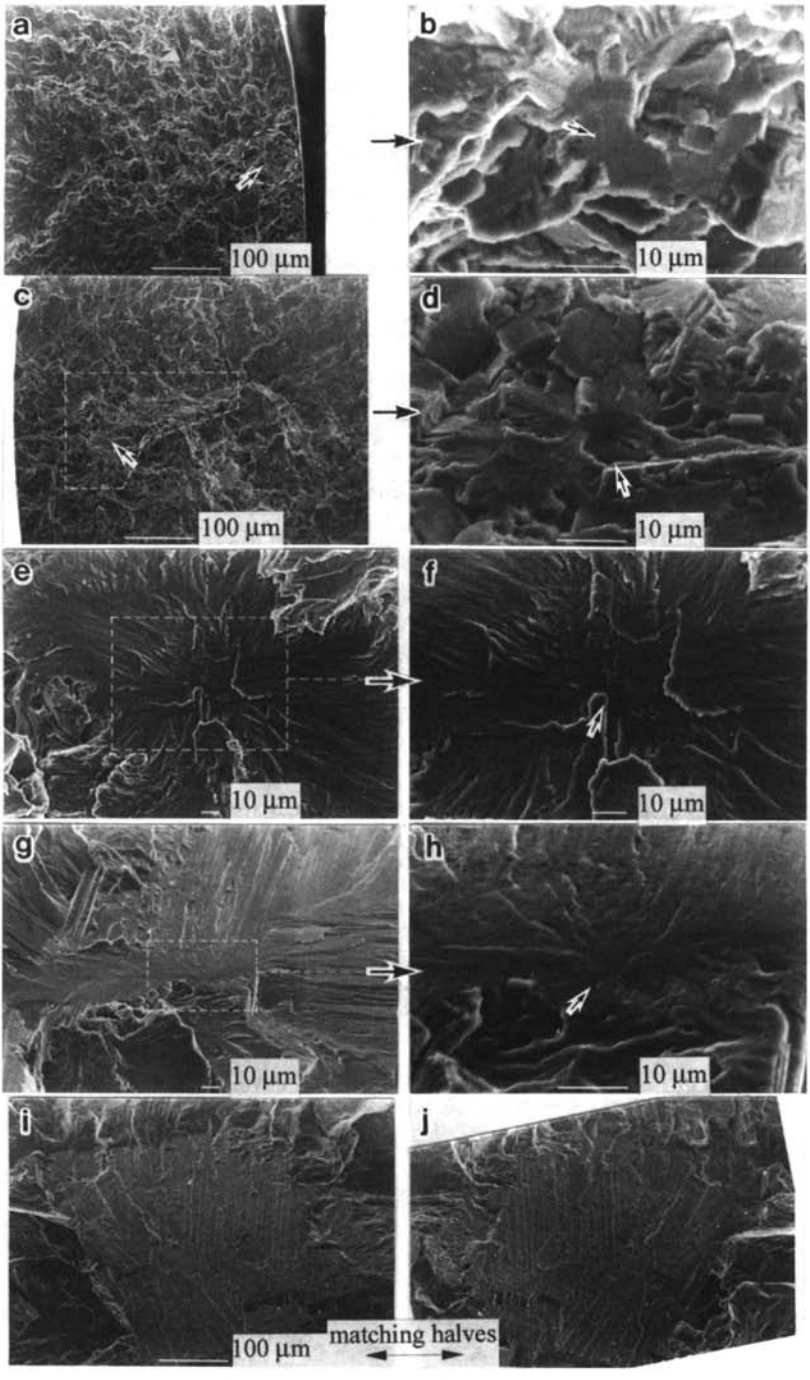

Figure 3 SEM photographs of fatigue crack initiation sites of the *annealed* materials: H1, σ_{max}=558 MPa (a, b), H2, σ_{max}=501 MPa (c, d), H3, σ_{max}=684 MPa (e, f), H4, σ_{max}=610 MPa (g, h) and H5, σ_{max}=750 MPa (i, j).

Subsurface Fatigue Crack Initiation Site

Morphology. No defect like inclusion or pore was detected at subsurface crack initiation sites. Figure 3 represents the SEM photographs of subsurface crack initiation sites for the *annealed* materials. Although subsurface crack initiation sites appear flat at low magnification, the subsurface crack initiation sites consist of one or more than two facets at higher magnification. In the H1 and H2, globular facets are observed in the site, as shown in Figure 3 (b) and (d). Each facet can be fitted to an α grain judging from its morphology and size. At lower stress level, a number of facets form an initiation site, as shown in Figure 3(d). As well as in the $\alpha+\beta$ *annealed* materials, the initiation sites in the β *annealed* ones (H3, H4 and H5) consist of one or more facets. Each facet can be fitted to an α platelet according to its morphology and size. The aligned facets are associated with the packet structure, and the boundary of packets might appear on the initiation site, as shown in Figure 3(f). A few cases exhibit a larger facet which reflects the prior-β structure, as shown in Figure 3 (i) and (j). Thus, the subsurface crack initiation site was a facet or its aggregate which was associated with the α grain structure in each material.

A facet or a part of facet at the initiation site appeared featureless. The facet except the featureless region gave an appearance like microcrack growth in a radial pattern from the featureless part. The results in the previous works [10,15] suggested that the facet was created by a process of microcrack growth involving a large number of cycles and not by an instantaneous spread of the original facet.

Sub-Cracks in fatigued specimen interior. In order to determine whether the origin was virtually an α grain cracking, sub-cracks (microcracks) were looked for in the longitudinal cross sections of fractured specimens. In each material, thus, sub-cracks were detected with various stress levels. In the β *annealed* materials, much less numbers of sub-cracks were detected. Most of the sub-cracks had a very small size with a few micron-meter in length. All sub-cracks were nucleated in the α phase, and in many cases they touch α-β interfaces as shown in Figure 4. The facet was identified as an α grain transgranular cracking in each material.

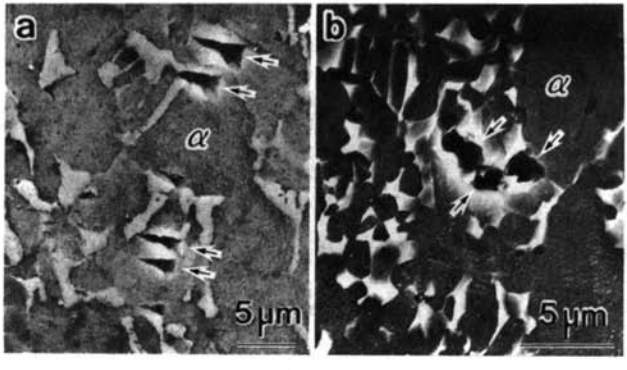

Figure 4 SEM micrographs of sub-cracks the *Normal* alloy at 4 K:
(a) *forged*, σ_{max}=1058 MPa and (b) *rolled*, σ_{max}=1306 MPa.

Dependence of Subsurface Crack Size on Stress Range

Evaluation by fs. Figure 5 shows the dependence of subsurface crack size, fs, on the peak cyclic stress for the materials studied. As the peak cyclic stress decreases, fs continuously increases from a few micron-meter to bigger than 100 μm. The evaluation by fs nicely exhibits the size change of subsurface crack initiation site with stress level, and fs is related unequivocally to the peak cyclic stress regardless of impurity content and microstructure.

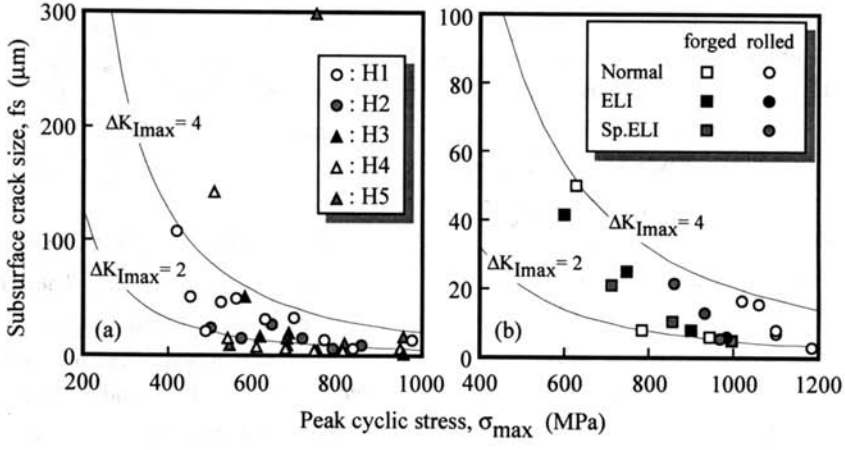

Figure 5 Relationship between subsurface crack size, fs, and peak cyclic stress at 77 K: (a) *annealed* materials and (b) *forged* and *rolled* materials.

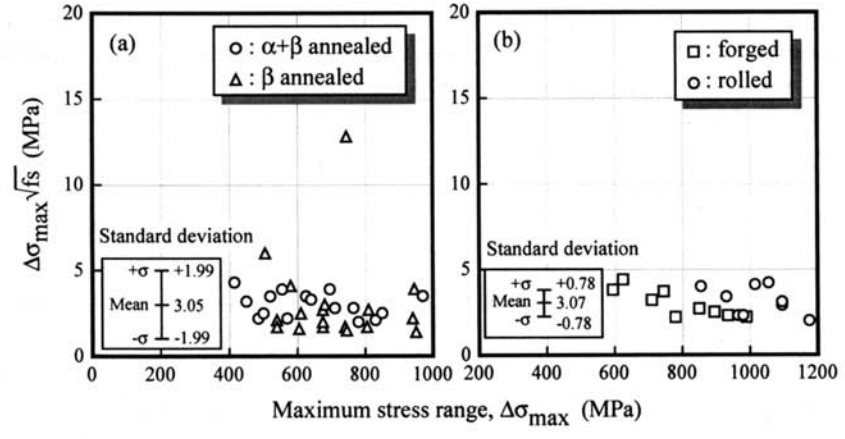

Figure 6 Relationship between maximum stress range, $\Delta\sigma_{max}$, and $\Delta\sigma_{max}\sqrt{fs}$: (a) *annealed* materials and (b) *forged* and *rolled* materials.

Critical condition of microcrack growth. The Stage I crack which is going to be selected for a main crack is always competitive with others and depends on the stress concentration at the

crack tip. For example, the fatigue limit of the material containing pre-existing defect such as inclusion was determined from the relationship between the defect size and threshold stress range.[17,18] In the present materials, the microcrack nucleated in an α grain did not always provided a critical main crack size. The microcrack needs to grow until it finally forms the initiation site with a critical size. Hence we evaluated the critical condition that a microcrack became a fatal crack in a given stress range.[10] The assumptions as follows were made for the simplification. At first, the parameter fs is equal to the crack-length of subsurface crack initiation site projected on the propagating plane. The subsurface crack initiation site is formed by the microcrack growth and is nucleus for the main crack. Although both of local and principal stresses take part in the formation of subsurface crack initiation site, the only principal stress controls the Stage I crack which becomes the main crack with size of fs. We conclude that the critical stress for the nucleus of main crack is almost equal to the principal stress. Then, an approximate equation to give the maximum stress intensity range, ΔK_{Imax}, at the subsurface crack tip is represented as follows.

$$\Delta K_{Imax} = A\, \Delta\sigma_{max}\sqrt{\pi\, fs} \qquad (1)$$

On the basis of the equation (1), Figure 6 rearranges the data in Figure 5 and shows the relationship between maximum cyclic stress range, $\Delta\sigma_{max}$, and $\Delta\sigma_{max}\sqrt{fs}$. The value of $\Delta\sigma_{max}\sqrt{fs}$ is mostly in a narrow range between 2 MPa$\sqrt{m}$ and 4 MPa$\sqrt{m}$. Thus, the stress dependence of the size can be fully explained by the present assumption. Here the coefficient A is roughly estimated to be 0.5 [18], although it depends on the shape and location of the initiation site. When the curves of ΔK_{Imax}=2 and 4 MPa$\sqrt{m}$ are overlaid in Figure 5, it is confirmed that almost all the data are included between the curves. Hence there is a critical condition, ΔK_{th}=constant, at any stress level where subsurface crack initiation occurs. Namely, the maximum stress range determines the critical size of microcrack at which a main crack starts to propagate. At higher peak stress level, only an α grain cracking can provide the size enough to trigger the microcrack growth. At lower peak stress level, on the other hand, one grain cracking is short and then the crack-spreading, multiple-cracking, and their coalescence occur to prove the size enough to grow as the Stage II crack.

Influence of Microstructure on S-N curves in Long-life Range

From the present S-N data, the influence of microstructure can be discussed from the two aspects; One is the influence of fatigue life at a given stress level, and the other is that on fatigue limit (10^7 cycles fatigue strength). A finer primary α grain size produces a longer-life where subsurface crack initiation occurs. For example, a rather sharp drop and/or "knee" point in the S-N curve for both H5 and *Sp.ELI* alloy shift to longer life than other curves in Figure 2, respectively. H5 has a finer α grain size than H3 and H5. *Sp.ELI* alloy also has a finer α grain size than other two alloys. However, finer α grain is not always effective on increasing 10^7 cycle fatigue strength, as shown in Figure 2. The *rolled* materials had much higher fatigue strength in the long-life range than the *forged* one, and their difference could not be explained in terms of tensile strength, macroscopic texture and α grain size.[15] In the forged materials, the primary α grains in a packet are believed to be crystallographically aligned and act as a single

path for dislocation motion as well as in the *β annealed* materials. H1 and H2 materials have equiaxed α grains, but the α grains might be partly aligned. In the *rolled* material, on the contrary, the crystallographical orientation between neighbor α grains might be much more random due to the hot-rolling. Thus, the *rolled* material is considered to provide an effective resistance to microcrack growth. In fact, each facet in a subsurface crack initiation site was inclined at random.[10] Furthermore, Williams and Luetjering reported that shorter slip length led to substantial improvements in fatigue strength for Ti-6Al-4V alloys.[19] Accordingly, the *rolled* material has a shorter slip length than the *forged* and *annealed* materials, which may introduce higher stress localization and facilitate crack initiation at a given applied stress.

From these consideration, we conclude that the fatigue strength of Ti-6Al-4V materials in the long-life range does not depend on the morphological differences itself in the microstructure. Namely, the finer α grain size or width produce a longer fatigue life at a low stress level. The orientation relationship between neighbor α grains could play the important role to increase fatigue strength in the long-life range where subsurface crack initiation occurs.

Summary

In high-cycle fatigue test at liquid nitrogen temperature, the subsurface crack initiation alloys and its microstructural origin were investigated on the different microstructures in Ti-6Al-4V alloys. The results are as follows;

(1) The difference in microstructure influenced the S-N curve in long-life range, which was related with subsurface crack initiation behavior.

(2) The subsurface crack initiation site consisted of one or more than two facets. The facet was fitted to an α grain transgranular cracking. The morphology and size of the subsurface crack initiation site were qualitatively assigned to the α microstructure in each material.

(3) As the maximum stress decreased, the size of subsurface crack initiation site increased. The size of subsurface crack initiation site was related unequivocally to the maximum stress regardless of material.

(4) The dependence of the initiation site size on the maximum stress range could be accounted for by an assumption that the microcrack growth criterion from Stage I crack to Stage II crack is determined by the critical condition, ΔK_{th}=constant.

References

1. O. Umezawa and K. Nagai, "A Review of Subsurface Crack Generation in High-cycle Fatigue for High Strength Alloys," ISIJ International, 37 (12) (1997), in printing.

2. A. Atrens et al., "Subsurface Crack Initiation in High Cycle Fatigue in Ti6Al4V and in a typical Martensitic Stainless Steel," Scripta Metall., 17 (1983), 601-606.

3. D. F. Neal and P. A. Blenkinsop, "Internal Fatigue Origins in α-β Titanium Alloys," Acta Metall., 24 (1976), 59-63.

4. J. A. Ruppen et al., "On the Process of Subsurface Fatigue Crack Initiation in Ti-6Al-4V," Fatigue Mechanisms, ASTM STP 675, ed. J. T. Fong (Philadelphia, PA: Ame. Soc. Test. Mater., 1979), 47-68.

5. J. A. Ruppen et al., "Subsurface Fatigue Crack Initiation of β-Annealed Ti-6Al-4V," Metall. Trans., 11A (1980), 1072-1075.
6. S. Adachi et al., " Influence of Microstructure and Mean Stress on Fatigue Strength of Ti-6Al-4V," Titanium Science and Technology, ed. G. Lutjering et al., vol. 4 (Oberursel, FRB: DGM, 1985), 2139-2146.
7. D. Eylon and B. Strope, "Fatigue Crack Initiation in Ti-6wt%Al-4wt%V Castings," J. Mater. Sci., 14 (1979), 345-353.
8. D. Eylon, "Fatigue Crack Initiation in Hot Isostatically Pressed Ti-6Al-4V Castings," J. Mater. Sci., 14 (1979), 1914-1922.
9. M. Hagiwara et al., "Effect of Microstructure on the Fatigue Behavior of Blended Elemental P/M Ti-6Al-4V Compacts," Tetsu-to-Hagane, 76 (1990), 2182-2189, in Japanese.
10. O. Umezawa et al., "Subsurface Crack Initiation in High Cycle Fatigue of Ti-6Al-4V Alloys at Cryogenic Temperatures," Tetsu-to-Hagane, 76 (1990), 924-931, in Japanese.
11. R. K. Steele and A. J. McEvily, "The High-Cycle Fatigue Behavior of Ti-6Al-4V Alloy," Engng. Fracture Mech., 8 (1976), 31-37.
12. K. Nagai et al., "Cryogenic Mechanical Properties of Ti-6Al-4V Alloys with Three Levels of Oxygen Content," ISIJ International, 31 (1991), 882-889.
13. M. Peters et al., "Influence of Microstructure on the Fatigue Behavior of Ti-6Al-4V," Titanium '80 Science and Technology, ed. H. Kimura and O. Izumi, vol. 3 (Warrendale, PA: The Metall. Soc. AIME, 1980), 1777-1786.
14. M. Peters et al., "Influence of Texture on Fatigue Properties of Ti-6Al-4V," Metall. Trans., 15A (1984), 1597-1605.
15. O. Umezawa and K. Ishikawa, "Phenomenological Aspects of Fatigue Life and Fatigue Crack Initiation in High Strength Alloys at Cryogenic Temperature," Materials Science and Engineering, A176 (1994), 397-403.
16. H. Yokoyama et al., "Distribution of Internal Crack Initiation Sites in High-cycle Fatigue for Titanium Alloys," ISIJ International, to be submitted.
17. H. Kitagawa et al., "Quantitative Analysis of Fatigue Process - Microcracks and Slip Lines Under Cyclic Strains," Fatigue Mechanisms, ASTM STP 675, ed. J. T. Fong (Philadelphia, PA: Ame. Soc. Test. Mater., 1979), 420-449.
18. Y. Murakami, "Quantitative Evaluation of Effects of Defects and Non-metallic Inclusions on Fatigue Strength of Metals," Tetsu-to-Hagane, 75 (1989), 1267-1277, in Japanese.
19. J. C. Williams and G. Luetjering, "The Effect of Slip Length and Slip Character on the Properties of Titanium Alloys," Titanium '80 Science and Technology, ed. H. Kimura and O. Izumi, vol. 1 (Warrendale, PA: The Metall. Soc. AIME, 1980), 671-681.